

NEW STRATEGIES FOR INTEGRATING PHOTOGRAMMETRIC AND GNSS DATA

C.M. Ellum and N. El-Sheimy

Department of Geomatics Engineering, University of Calgary, 2500 University Drive NW, Calgary, AB, T2N 1N4
cmellum@ucalgary.ca, naser@geomatics.ucalgary.ca

Inter-Commission Working Group V/I

KEY WORDS: Photogrammetry, Adjustment, Estimation, GNSS, Aerial, Multi-sensor

ABSTRACT:

GNSS-controlled photogrammetry is a mature technology that has found near universal acceptance in the aerial mapping community. The current strategy for integrating photogrammetric and GNSS data is to first process the GNSS data using a stand-alone kinematic Kalman filter processor, and then to use the resulting positions as parameter observations in a photogrammetric bundle adjustment. The utility of this implementation has been well-proven; however, there has been little research into other integration strategies. In this paper, investigations are made into some alternative integration approaches. Focus is given to two techniques: first, an approach with improved information-sharing between the GNSS and photogrammetric processors, and second, a combined least-squares adjustment of the raw GNSS and photogrammetric measurements. After providing background on the existing integration strategies, the new approaches are introduced and detailed. Tests are made using a standard aerial block, results from which appear to indicate that the new techniques do not improve mapping accuracy over the conventional approach. The new techniques, however, may improve GNSS positioning accuracy or enable some more unique network configurations.

1 BACKGROUND

Of all the groups that have found uses for Global Navigation Satellite Systems (GNSS), there can be few that have embraced them as enthusiastically and universally as the aerial photogrammetric mapping community. Not only was this community one of the first to identify the theoretical advantages GNSS could provide, they were also one of the first to put it into operational practice. Indeed, from shortly after the first GNSS system became operational it would have been near impossible to find any aerial photogrammetric mapping company whose operations were not centred around kinematic GNSS controlled photogrammetry.

Unfortunately, the integration of GNSS with photogrammetry is somewhat a victim of its own success. The technique first used for the integration was so successful that there has been virtually no research into additional integration strategies.

This paper reviews the existing integration strategies for integrating photogrammetric and GNSS data, and introduces some alternative approaches. Focus is given to two techniques: first, an information-sharing approach between GNSS and photogrammetric processors, and second, a combined least-squares adjustment of the photogrammetric and GNSS measurements.

2 EXISTING INTEGRATION STRATEGIES

In photogrammetric literature, two techniques for combining GNSS and photogrammetric data streams have been identified. The first envisioned, where GNSS-derived positions are included in bundle adjustment via position observations, has been used near-universally and without modification ever since. The second technique, a development on the positions-observation approach, has seen only limited use.

2.1 Including GNSS data via position observations

The integration of GNSS and photogrammetric data is almost always done by incorporating GNSS position observations in

photogrammetric bundle (block) adjustments. This is essentially a two-step technique. In the first step, raw GNSS measurements are processed in a kinematic GNSS Kalman filter, yielding estimates of antenna position and position covariance at the GNSS measurement epochs. Using a linear or other low-order polynomial, position and covariance corresponding to the exposure times are then interpolated from these positions. In the second step, the estimates of exposure-station antenna position are used in a photogrammetric adjustment as position parameter observations. The nominal form of these equations is

$$\mathbf{r}_a^M = \mathbf{r}_c^M + \mathbf{R}_c^M \mathbf{r}_a^c, \quad (1)$$

where \mathbf{r}_a^M is the GNSS antenna position observation that is related to the camera perspective centre \mathbf{r}_c^M through the camera-GNSS antenna lever-arm \mathbf{r}_a^c . \mathbf{R}_c^M is the rotation matrix that aligns the reference frame of the camera with that of mapping space.

When this integration strategy was first devised, receivers and ambiguity resolution techniques were less advanced than they are today. As a result, the ambiguities resolved in the GNSS Kalman filter were incorrect more often, leading to incorrect position estimates. To combat this, Equation (1) was augmented to include position bias and time-dependent linear drift terms, leading to the form of the equation that is used near-universally today,

$$\mathbf{r}_a^M = \mathbf{r}_c^M + \mathbf{R}_c^M \mathbf{r}_a^c + \mathbf{b}_a^M + \mathbf{d}_a^M (t - t_0). \quad (2)$$

The position bias and drift terms, denoted by \mathbf{b}_a^M and \mathbf{d}_a^M , respectively, are estimated in the adjustment. Normally, each strip of imagery gets its own set of these parameters. If ground control is also used in the adjustment, then these two parameters can also account for inconsistencies between the datum and the GNSS positions.

The flow of information in the position-observations integration strategy is illustrated in Figure 1. More information on this technique can be found in Ackermann, 1992 or Mikhail et al., 2001.

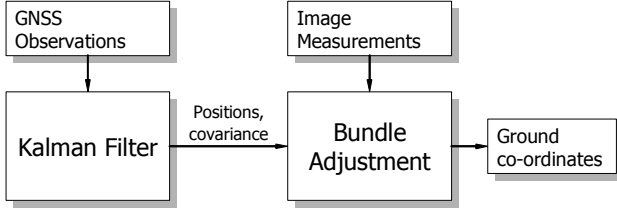


Figure 1: Position-observations technique

A minor variation on the position-observations integration strategy is to re-parameterise the image measurement equations so that they are explicitly functions of the GNSS antenna positions (Ellum, 2001). This is done by substituting

$$\mathbf{r}_c^M = \mathbf{r}_a^M - \mathbf{R}_c^M \mathbf{r}_a^c, \quad (3)$$

into the forward conformal transformation relating object space co-ordinates of a point with its image measurements,

$$\mathbf{r}_p^M = \mathbf{r}_c^M + \mu \mathbf{R}_c^M \mathbf{r}_p^c, \quad (4)$$

yielding

$$\mathbf{r}_p^M = \mathbf{r}_a^M + \mathbf{R}_c^M (\mu \mathbf{r}_p^c - \mathbf{r}_a^c), \quad (5)$$

By rearranging Equation (5), the reverse transformation is found to be

$$\mathbf{r}_p^c = \mu^{-1} [\mathbf{R}_c^M (\mathbf{r}_p^M - \mathbf{r}_a^M) + \mathbf{r}_a^c]. \quad (6)$$

Finally, eliminating the third equation in the above system of equations results in image measurement equations that are explicitly functions of the GNSS antenna positions,

$$\begin{aligned} x_p &= \frac{r_{11}X_{a/P} + r_{12}Y_{a/P} + r_{13}Z_{a/P} + x_a}{r_{31}X_{a/P} + r_{32}Y_{a/P} + r_{33}Z_{a/P} + z_a} \\ x_p &= \frac{r_{21}X_{a/P} + r_{22}Y_{a/P} + r_{23}Z_{a/P} + y_a}{r_{31}X_{a/P} + r_{32}Y_{a/P} + r_{33}Z_{a/P} + z_a} \end{aligned}, \quad (7)$$

These equations are virtually the same as the normal image measurement collinearity equations, with the only differences being that the camera co-ordinates have been replaced by the GNSS antenna co-ordinates, and both the numerator and denominator have had components of the GNSS-camera lever-arm added to them. Terming these equations collinearity equations would, however, be a misnomer, as the GNSS antenna is almost certainly not collinear with the object space point and its corresponding image measurement.

The revised image measurement equations have a number of advantages. First, the GNSS antenna position observation reduces to a direct parameter observation, $\mathbf{r}_a^M = \hat{\mathbf{r}}_a^M$. Secondly, multiple camera systems need only be referenced to a single position. This reduces the number of parameters in the adjustment, and more closely corresponds to the true imaging situation.

2.2 Modelling GNSS satellite range errors

To the authors' knowledge, only one other technique of integrating GNSS and photogrammetric data has been investigated or implemented. This was done at the University of Hanover and Geo++ GmbH in the mid-nineties. In their ingenious approach, outlined in Jacobsen and Schmitz (1996) and Kruck et al. (1996), constant satellite-to-exposure station range corrections are estimated within the bundle adjustment for each GNSS satellite whose ambiguity was not reliably fixed in the kinematic GNSS processor. The development of this technique begins with the linearised GNSS range observation equations, where the addi-

tional range corrections $\Delta \mathbf{l}$ are explicitly separated from the range measurements \mathbf{l} ,

$$\mathbf{l} + \Delta \mathbf{l} = \mathbf{A} \mathbf{x}. \quad (8)$$

where \mathbf{x} is the vector of GNSS co-ordinates and \mathbf{A} is the GNSS design matrix (i.e., the Jacobian of the double-difference GNSS observations with respect to the antenna co-ordinates). The least squares solution to Equation (9) is

$$\mathbf{x} = (\mathbf{A}^T \mathbf{P} \mathbf{A})^{-1} \mathbf{A}^T \mathbf{P} \mathbf{l} + (\mathbf{A}^T \mathbf{P} \mathbf{A})^{-1} \mathbf{A}^T \mathbf{P} \Delta \mathbf{l}. \quad (9)$$

This equation has two terms: the first is the GNSS co-ordinate vector that would be solved for in the absence of the $\Delta \mathbf{l}$ range corrections, and the second is a vector of co-ordinate corrections that results because of these range corrections. This second term is introduced into the bundle adjustment's GNSS position observation equation,

$$\mathbf{r}_a^M = \mathbf{r}_c^M + \mathbf{R}_c^M \mathbf{r}_a^c + (\mathbf{A}^T \mathbf{P} \mathbf{A})^{-1} \mathbf{A}^T \mathbf{P} \Delta \mathbf{l}. \quad (10)$$

The $\Delta \mathbf{l}$ range corrections are then added to the bundle adjustment as unknown parameters. The design and weight matrices are provided to the adjustment by the kinematic GNSS processor.

By comparing Equation (2) with Equation (10), it is apparent that the range corrections are effectively replacing the shift and drift terms from the conventional approach. The difference between the two approaches is that the GNSS errors are now being modelled and compensated for in measurement-space rather than in object-space. The actual integration, however, is still done in position-space.

This integration technique has several advantages over the traditional position observation GNSS/photogrammetry integration strategy, yet it is not quite the "rigorous" integration claimed. Improvements over the traditional approach include:

- the actual GNSS errors are better considered
- the number of unknowns is (in general) reduced
- no cross-strips are required
- GNSS errors can better be separated from datum and interior orientation parameters

In spite of these advantages it is, however, important to note that the actual GNSS ranges themselves are not used in the adjustment, and the integration is still done in object space. Also, the sharing between the GNSS and photogrammetric processors is, like in the conventional approach, only in one direction. In fairness, the creators of the technique do note that "re-substitution of the [range correction] terms [into the GNSS processor] is feasible"; however, they conclude that "it is not of much interest as the [GNSS] processing techniques improve" (Jacobsen & Schmitz, 1996).

There are a number of practical, implementation-related, obstacles that need to be overcome with this integration strategy. Firstly, the GNSS design matrices must be transferred between the photogrammetric and GNSS processors. Most GNSS processors do not output such information, and so a customised processor is required. Secondly, there is the problem of determining which GNSS position observations need to have the additional range corrections applied, and to which positions each range correction applies. This bookkeeping must be performed in the GNSS processor, and again, transferred to the adjustment.

3 ALTERNATIVE INTEGRATION STRATEGIES

There are three alternative GNSS/photogrammetric strategies that are, conceptually, straightforward developments of existing techniques. These are presented below.

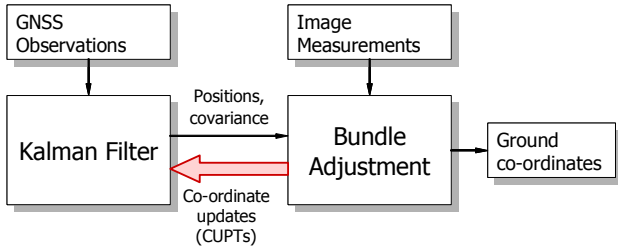


Figure 4: Inter-processor communication

3.1 Inter-processor communication

Perhaps the most basic alternative integration strategy is one where the existing position-observations approach is modified so that photogrammetric bundle adjustment feeds co-ordinate updates (CUPTs) back into the GNSS Kalman filter. In this technique, shown in schematic form in Figure 4, the GNSS processor no longer works in isolation from the photogrammetric processor; instead, it is “aided” by positions output by the bundle adjustment.

These positions from the bundle adjustment are incorporated into the Kalman filter using simple state-observation equations. Obviously the exact form of these equations depends on the co-ordinate frames used by the two processors and the type of Kalman-filter. However, if, for example, both the bundle adjustment and navigation processing are done in the *e*-frame, and if the Kalman filter is a total-state filter, then the CUPT observation equation is

$$\mathbf{r}_c^e + \mathbf{R}_c^e \mathbf{r}_a^e = \mathbf{x} \tag{11}$$

In this equation, \mathbf{x} is the block of the Kalman filter’s state vector corresponding to the positions. The \mathbf{r}_c^e and \mathbf{R}_c^e terms, respectively the exposure station’s position and attitude, are provided by the bundle adjustment. This weight of the observation is equivalent to the exposure stations covariance, $\mathbf{C}_{\mathbf{r}_c^e}$, also output by the adjustment.

A minor complication in this approach is that the exposure times and, consequently, the CUPT filter updates likely do not coincide with GNSS measurements epochs. However, this is easily handled by having the Kalman Filter predict up to the time of the CUPT before performing the measurement update, as shown in the figure below.

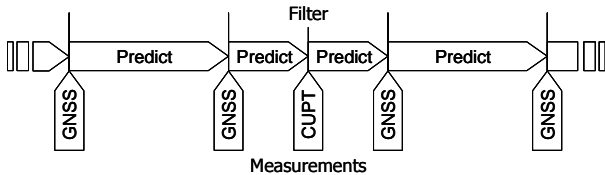


Figure 2: Operation of the GNSS Kalman filter

This integration approach’s primary advantage is its ease-of-implementation: the bundle adjustment already outputs the positions and covariance of the exposure stations, and the Kalman filter requires only minimal (if any) changes to incorporate the CUPTs. Unfortunately, the integration is still only at position level.

3.2 Combined adjustment

Integration of the GNSS and photogrammetric data streams can be done at the measurement level using a combined adjustment. In this approach, both the image measurements and the raw GNSS code and carrier phase range observations are used in a

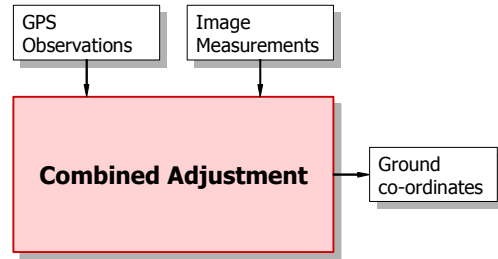


Figure 3: Combined adjustment

single simultaneous least-squares adjustment. A conceptual overview of the combined adjustment is shown in Figure 3.

A combined adjustment integration approach has a number of benefits. Practically, it simplifies the processing of the two data streams, as only a single software package is required. It also enables GNSS data to be used when data from less than four satellites is available, which is not the case in current integration strategies. While such a feature is not particularly relevant for airborne mapping, it does have applicability in terrestrial mapping systems. A combined adjustment also allows for a non-fixed GNSS base station. Instead, control for the entire network’s datum can come from ground control points observed in the images. Finally, the most anticipated benefit is improved reliability of the entire integration process; in particular, an improved ability to detect errors in the GNSS measurements.

Of course, the combined adjustment has several disadvantages. For instance, it is not possible to make use of a kinematic model as is done in a GNSS Kalman filter. Also, implementing the combined adjustment requires significant effort. Finally, there are important and as yet unresolved issues with regards to the correct relative weighting of the different observation types.

3.2.1 Parameterisation of the exposure positions

Obviously, to include both the GNSS and image measurements in the adjustment there must be some connectivity between them. The necessary connections are provided through the exposure station positions, from which both types of observations are made. The actual implementation of the adjustment depends, however, on how the exposure positions are parameterised. For this there are three options:

1. Express the camera position in terms of the GNSS antenna co-ordinates \mathbf{r}_a^M , and modify the image measurement equations accordingly.
2. Express the GNSS antenna position in terms of the camera co-ordinates \mathbf{r}_c^M , and modify the GNSS measurement equations accordingly.
3. Include both GNSS antenna and camera co-ordinates in the adjustment and add camera-antenna lever-arm constraint equations. In their simplest form, these constraints would be $\mathbf{r}_a^c = \mathbf{R}_M^c (\mathbf{r}_a^M - \mathbf{r}_c^M)$.

Of these three options, the first is preferable. As was shown in Section 2.1, modifying the image measurements so that they are functions of the antenna positions is straightforward. The same cannot be said for modifying the GNSS observation equations to be functions of the camera positions, making the second option undesirable. The final option allows both the conventional image and GNSS measurement equations to be used, but otherwise increases the complexity and computational requirements of the adjustment; thus, it is also undesirable.

3.2.2 GNSS observation equations Expressing the exposure positions in terms of the antenna positions enables the standard form of the GNSS observation equations to be used. It is, of course, possible to include any type of GPS observation, but the most commonly used GNSS observations are undifferenced code

range measurements and double-differenced code and carrier phase measurements. The observation equation for the former is

$$p = |\mathbf{r}_{SV} - \mathbf{r}_a| + c\Delta t_{rx} = |\mathbf{r}_{a/SV}| + c\Delta t_{rx}, \quad (12)$$

with p the code range measurement, \mathbf{r}_{SV} the position of the satellite, c the speed of light, and Δt_{rx} the bias of the GNSS receiver's clock. This last term is added to the combined adjustment as an unknown parameter, with normally one clock offset required for each epoch of GNSS observations. The observation equation for double-difference code range measurement is found by twice differencing Equation 12 across two antennas and two satellites. Explicitly, this is

$$\begin{aligned} \Delta\nabla p &= (|\mathbf{r}_b - \mathbf{r}_m| - |\mathbf{r}_i - \mathbf{r}_m|) - (|\mathbf{r}_b - \mathbf{r}_a| - |\mathbf{r}_i - \mathbf{r}_a|) \\ &= (|\mathbf{r}_{m/b}| - |\mathbf{r}_{m/i}|) - (|\mathbf{r}_{a/b}| - |\mathbf{r}_{a/i}|) \end{aligned} \quad (13)$$

The double-difference code range measurement is denoted by $\Delta\nabla p$, and the master station and exposure position by m and a , respectively. The base and other (i^{th}) satellite are indicated by b and i . Unlike the undifferenced code observations, the double-difference code observations do not require the addition of any parameters to the adjustment. Finally, for the double-difference carrier phase measurements the observation equation is

$$\Delta\nabla\Phi = (|\mathbf{r}_{m/b}| - |\mathbf{r}_{m/i}|) - (|\mathbf{r}_{a/b}| - |\mathbf{r}_{a/i}|) + \Delta\nabla N, \quad (14)$$

where $\Delta\nabla\Phi$ indicates the double-difference phase measurement, and $\Delta\nabla N$ the double-difference phase ambiguity for this master-base/satellite pair. The ambiguity is included in the adjustment as a parameter, with one ambiguity required for each continuously tracked satellite.

3.2.3 Normal matrix structure The complete normal matrix for a combined adjustment incorporating image measurements, a camera calibration, undifferenced GNSS code ranges, and double-difference GNSS carrier phases resembles

$$\mathbf{N} = \begin{bmatrix} \mathbf{N}_{EOP} & \sim & \sim & \sim & \sim \\ \sim & \mathbf{N}_{IOP} & \mathbf{0} & \mathbf{0} & \sim \\ \sim & \mathbf{0} & \mathbf{N}_{\Delta t_{rx}} & \mathbf{0} & \mathbf{0} \\ \sim & \mathbf{0} & \mathbf{0} & \mathbf{N}_{\Delta\nabla N} & \mathbf{0} \\ \sim & \sim & \mathbf{0} & \mathbf{0} & \mathbf{N}_{pts} \end{bmatrix}. \quad (15)$$

This matrix is divided into three sections, one each for the photogrammetric, GNSS, and tie/pass point co-ordinate parameters, respectively. The photogrammetric section consists of blocks for the exterior and interior orientation parameters: \mathbf{N}_{EOP} and \mathbf{N}_{IOP} , respectively. The GNSS block includes blocks for the receiver clock offsets, $\mathbf{N}_{\Delta t_{rx}}$, and double-difference ambiguities, $\mathbf{N}_{\Delta\nabla N}$. The ' \sim ' indicates non-zero off-diagonal blocks.

3.3 Combined filter

A final integration option, depicted in Figure 5, is a combined Kalman filter. The advantage of this approach is that a kinematic model relating GNSS navigation quantities (positions, velocities, accelerations) can be used. Unfortunately, because the filter's state vector would have to include all of the photogrammetric and tie/pass point parameters, in addition to the GNSS navigation states, the computational requirements of this approach would be enormous. It is also significantly more difficult to implement than either of the two previous approaches.

4 TESTING OF ALTERNATIVE STRATEGIES

The inter-processor communication and combined adjustment integration approaches have been implemented, and tests using

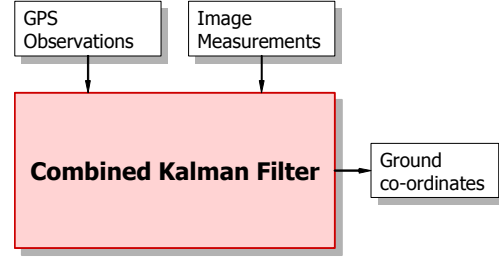


Figure 5: Combined filter

the two methods are described below. However, as was just indicated, the combined Kalman filter is disadvantaged by computational requirements and implementation complexity, and was thus neither implemented nor tested.

4.1 Data set description

The data set used for testing consisted of a block of 84 aerial images captured at a photo scale of approximately 1:5,000. Image acquisition was done using a conventional 9"×9" frame camera with a 6" focal length. Co-ordinates were available for 17 ground points; these points were treated as check points in the tests that follow. GPS data at 2Hz was collected on the aeroplane and at a master station located approximately 24km from the centre of the block. Dual-frequency data was available at both stations but the tests that follow use data on L1 only. The arrangement of the data set's exposures and ground points can be seen in Figure 6.

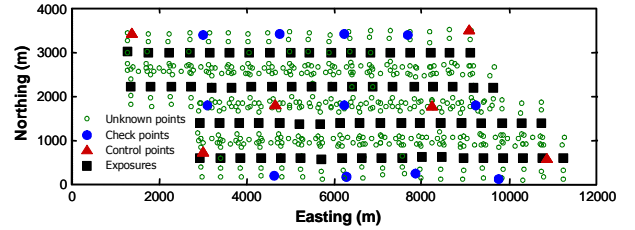


Figure 6: Test field

Unfortunately, there was an unknown but appreciable translation between the datum of the data set's ground points and the datum used by the GPS (WGS84). This included, but was not limited to, the geoid height, as only orthometric heights were available for the check points.

4.2 Conventional processing

The first tests performed with the data used conventional processing strategies, and were done to establish the noise level inherent in the network. Results from these tests will act as the basis of comparison for the tests of the new integration techniques that follow. The noise level in the network, due in turn to the image measurement noise, was observed using two configurations: a network controlled using ground points, and a network controlled using the best available GPS-derived exposure station positions. For the ground controlled network, 6 well-distributed points were selected to act as control and the remaining 11 points were used as check points. Figure 6 shows the distribution of these points. For the GPS-controlled network, exposure station position observations were generated by a commercial GPS processor using dual-frequency data. Ambiguities were reported as fixed for all stations. All 17 available check points were used to generate the statistics.

The results for these two network configurations are listed in Table 1. The results from both configurations indicate that there is about 10cm of horizontal and 20-25cm of vertical noise in the network. These are, it is believed, the highest-achievable accuracies reasonably available from the data.

Table 1: Check-point error standard deviations for nominal network configurations (m)

Datum Control	Horizontal	Vertical
Ground control points	0.11	0.22
Best-available GPS position observations	0.11	0.26

4.3 Feedback filter

Testing using the feedback-filter integration approach will focus on both the check-point accuracy and on the accuracy of the GNSS (GPS) positioning. In the latter case, dual-frequency, integer ambiguity positions from a commercial GNSS processor were used as the basis of comparison. The processor used for the tests, however, was an all new GNSS processor designed specifically for the task. As noted above, only single-frequency data was used in the tests. Also, only real (float) ambiguities were estimated.

In the first set of tests done using the feedback approach, no accuracy improvement was seen in either the GPS positions or the check-point positions. In both cases accuracy after the CUPT feedback was the same as before the CUPT feedback. Given the benign nature of the test network – i.e., its clean GPS data and good imaging-geometry – this was not entirely unexpected. What was a surprise, however, was that the check-point accuracies, shown in Table 2, were at the same level as the nominal tests of Table 1. In other words, using dual-frequency data and ambiguity fixing with the conventional positions observations approach did not provide any improvement to using single-frequency data and real ambiguities. This implies that difficult and potentially unreliable integer-ambiguity fixing need not always be attempted.

Table 2: Check-point error standard deviations for feedback filter using clean GPS data (m)

	Horizontal	Vertical
Before CUPTS	0.11	0.20
After CUPTS	0.11	0.20

To simulate a more challenging data set, a second test was done in which a cycle-slip was induced on the base satellite in between two of the strips, causing the GNSS filter’s ambiguity estimates to be reset. In this case, the feedback of the CUPTS into the GNSS processor did provide a small improvement in the accuracy of the GPS positions that followed the reset. This improvement is shown in Table 3. Graphically, the effect of the CUPTS on the GPS position errors can be seen in Figures 7 and 8. In Figure 8, the highlighted discontinuity in the position errors is due to the first CUPT following the filter reset.

Table 3: GPS position error statistics, cycle-slip in GPS data

Statistic	Before CUPTS	After CUPTS
Std. Dev. (m)	0.17	0.13
RMSE (m)	0.18	0.16

Unfortunately, the improved GPS positioning did not translate into improved photogrammetric mapping accuracy. Here again, however, the reason seems to be that the strength of the photogrammetric block is such that the degraded, cycle-slipped positions do not effect results even before the CUPTS are applied. As can be seen in Table 4, accuracies both before and after the

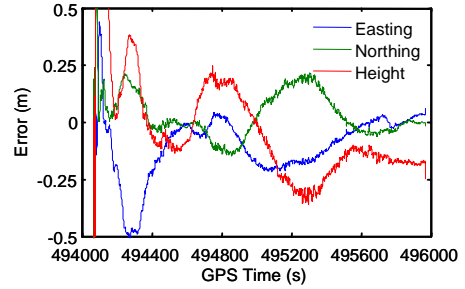


Figure 7: GPS position errors before CUPT feedback

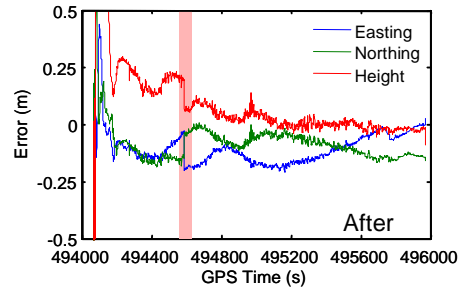


Figure 8: GPS position errors after CUPT feedback

CUPT-improved GPS positions were used in the bundle adjustment were at the same level as the best possible accuracies expected from the network.

Table 4: Check-point error standard deviations for feedback filter using cycle-slip degraded GPS data (m)

	Horizontal	Vertical
Before CUPTS	0.14	0.16
After CUPTS	0.09	0.21

4.4 Combined adjustment

The combined adjustment integration technique was tested by comparing it to the existing technique of position observations. The position observations for these tests were generated using the adjustment program in the same configuration as in the combined adjustment, except that the image measurements were not included. The positions generated as such have been found to have similar accuracy to those generated by a commercial kinematic processor using the same type of observations.

An important consideration in adjustments incorporating multiple observation types is the relative weighting of the different observation groups. In the tests that follow, the image measurement standard deviation was held constant at values believed to be reasonable for the analytical plotter and operator used for the data collection. Conversely, the weight of the either the raw GPS measurements or the GPS-derived position observations were varied until the *a posteriori* variance factor for each observation type was approximately equal to 1.0. This approach appeared to lead to the best possible results.

Results are shown below for tests using double-difference GNSS code ranges and carrier phases. Results from tests using undifferenced code ranges can be found in Ellum and El-Sheimy, 2005.

4.4.1 Double-difference code ranges The first type of GNSS measurements used in the combined adjustment were double-difference code-ranges, with the results being shown in Table 5. Two obvious observations can be made from these results: first, the combined adjustment offers no improvement in accuracy over the position observations approach, and second, in either case accuracies are far from the best available from the network.

An additional observation made during the tests was the importance of including the position observations' covariance information. If the position observations were included with variances only, then horizontal and vertical accuracies were over 10% and 25% worse, respectively.

Table 5: Check-point error standard deviations for combined adjustment using double-difference code-ranges (m)

	Horizontal	Vertical
Combined adjustment	0.50	0.87
Position observations	0.52	0.92

4.4.2 Double-difference carrier-phases The next test of the combined adjustment used both double-differenced GNSS code ranges and carrier-phases. Real (float) ambiguities were estimated in the adjustment. Table 6 shows the result from this test. Again, the combined adjustment and position observations methods provide results that are effectively the same. Notably, results in both cases are only slightly worse than the best possible results available from the network.

Table 6: Check-point error standard deviations for combined adjustment using double-difference code ranges, carrier-phases, and real ambiguities (m)

	Horizontal	Vertical
Combined adjustment	0.10	0.31
Position observations	0.11	0.26

With the float ambiguity solutions performing so well, it was not expected that fixing the ambiguities would significantly impact positioning accuracy. This was indeed the case, with the check point error's standard deviation being within 1cm of that of the float ambiguity results. As was the case with the feedback-filter approach, this appears to indicate that integer ambiguity fixing need not always be attempted.

4.4.3 Unusual network configurations A benefit of the combined adjustment is that it allows for more flexibility in how the data can be used. Two examples identified earlier were having a non-fixed GNSS master station and using less than four satellites. Results from both configurations are shown below in Table 7. For the first set of results in this table the datum was controlled by a single ground control point located near the centre of the block. Accuracies in this case were as good as the best possible from the network. This configuration neatly avoids any inconsistencies between the GNSS and photogrammetric control datums. Of course, should the differences between the two datums be too large then this would cause errors in relative GNSS baselines implicitly used in the combined adjustment.

Table 7: Check-point error standard deviations for combined adjustment used in unusual configurations (m)

Configuration	Horizontal	Vertical
Datum control by a single ground control point	0.13	0.21
GNSS measurements used from only 3 satellites	0.53	0.49

5 CONCLUSIONS AND OUTLOOK

The most obvious conclusion that can be drawn from the tests in the previous section is that, for a standard aerial block, at least, the new integration techniques appear to offer no improvement in mapping accuracy over the conventional position observations technique. However, even without improved mapping accuracy, the new integration techniques still have a number of advantages over the traditional position-observations technique.

In particular, the feedback filter has the potential to improve GNSS positioning results, and the combined adjustment enables more flexible processing options. It should also be noted that the data set used for the tests in this paper was fairly benign, and a more challenging data set – in particular, a terrestrial mobile-mapping data set – may lead to different conclusions. Finally, the important question of whether the new integration techniques provide improved reliability has not yet been addressed.

An additional conclusion, unrelated to the integration approach, is that results using double-differenced single-frequency GNSS carrier phase data can be as accurate as those determined from using dual-frequency data with ambiguity fixing. This implies that difficult and potentially unreliable integer-ambiguity fixing need not always be attempted.

The implementation of both the feedback filter and combined adjustment could be improved from how it was done here. For example, in current feedback filter, the exchange of information between the GNSS Kalman filter and the bundle adjustment is done manually. This process could, however, be automated, and the adjustment made to run sequentially, rather than just repeating the batch adjustment as is currently done. The combined adjustment could also be improved. Currently, it only uses the (interpolated) GNSS measurements that correspond to the exposure positions. It is possible, though, to use all the GNSS measurements. Of course, this would result in additional position parameters for each epoch of measurements used, but these additional positions could be eliminated from the normal system of equations during their formation. Thus, a significant increase in computational load would not be incurred.

The combined adjustment, in particular, opens up a number of avenues for further research. One interesting possibility would be to estimate GNSS measurement biases within the adjustment. The estimation of such biases could be improved both by having the GNSS positions tied together through the photogrammetric observations, and by controlling the datum by photogrammetric ground control. An obvious type of bias that could be estimated in this manner is undifferenced or double-difference residual zenith tropospheric delays. Even more ambitiously, attempts could be made to estimate undifferenced carrier-phase ambiguities.

REFERENCES

- Ackermann, F., 1992. Kinematic GPS control for photogrammetry. *Photogrammetric Record*, 14(80), pp. 261–276.
- Ellum, C.M., 2001. *The Development of a Backpack Mobile Mapping System*. M.Sc. Thesis, University of Calgary, Calgary, Canada.
- Ellum, C.M. and El-Sheimy, N., 2005. Integrating photogrammetry and GPS at the measurement-level. *Proceedings of ION GNSS 2005*. September 13-16, Long Beach, CA, USA.
- Jacobsen, K. & M. Schmitz, 1996. A new approach of combined block adjustment using GPS-satellite constellation. *Proceedings of the 18th ISPRS Congress*. July 9-19. Vienna, Austria. International Archives of Photogrammetry, Vol. 31.
- Kruck, E., G. Wübbena & A. Bagege, 1996. Advanced combined bundle block adjustment with kinematic GPS data. *Proceedings of the 18th ISPRS Congress*. July 9-19. Vienna, Austria. International Archives of Photogrammetry, Vol. 31.

ACKNOWLEDGEMENTS

Camal Dharamdial at The Orthoshop is thanked for providing the test data set. Funding for this research was provided by the Killam Trusts and the Natural Sciences and Engineering Research Council of Canada (NSERC).